Journal of Materials Chemistry

www.rsc.org/materials

Volume 22 | Number 33 | 7 September 2012 | Pages 16659–17350

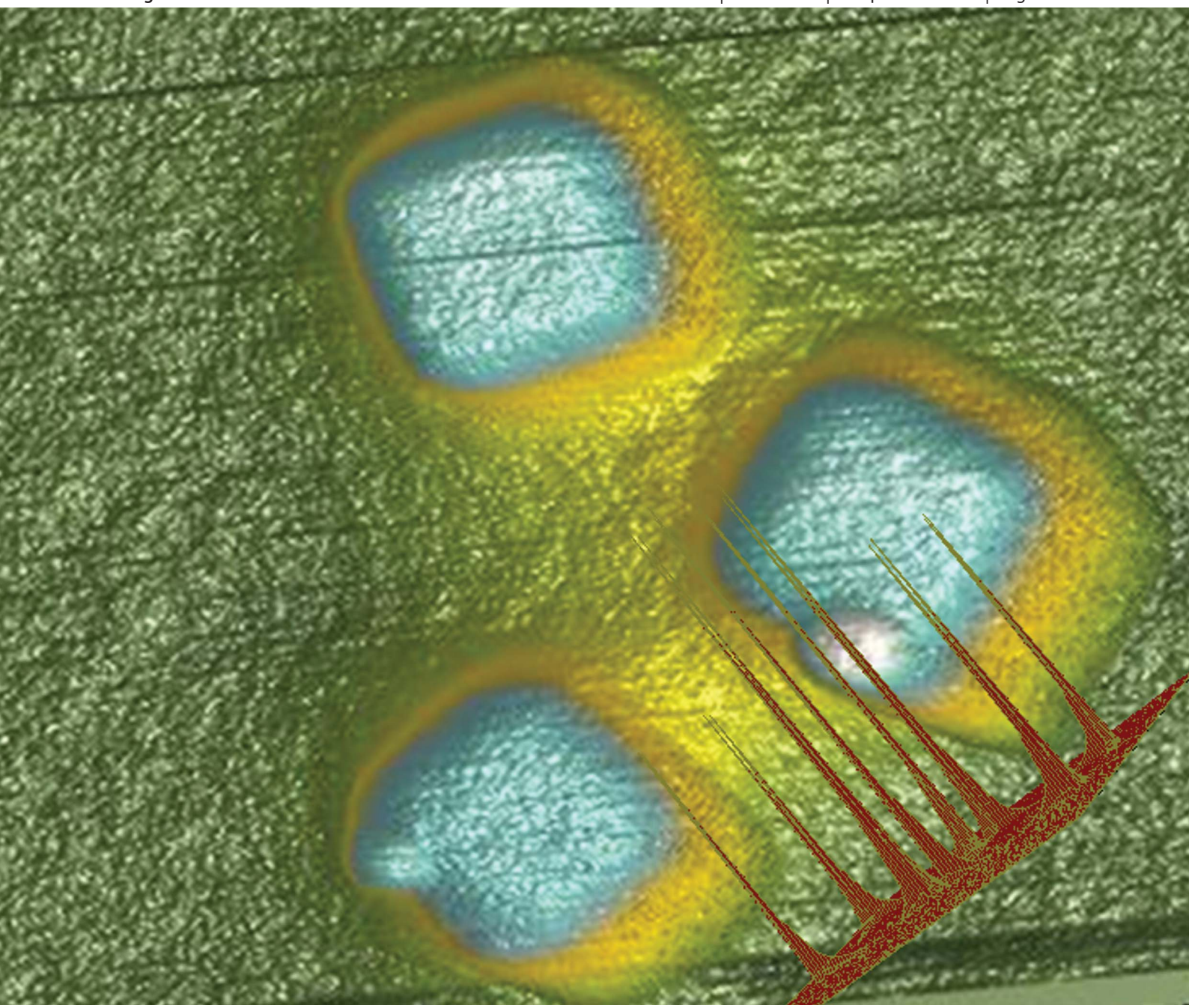

ISSN 0959-9428

RSC Publishing

PAPER

Vladimir V. Tsukruk *et al.*

The unusual fluorescence intensity enhancement of poly(*p*-phenyleneethynylene) polymer separated from the silver nanocube surface by H-bonded LbL shells

0959-9428(2012)22:33;1-D

Journal of Materials Chemistry

Dynamic Article Links

Cite this: J. Mater. Chem., 2012, 22, 16745

www.rsc.org/materials

PAPER

The unusual fluorescence intensity enhancement of poly(*p*-phenyleneethynylene) polymer separated from the silver nanocube surface by H-bonded LbL shells

Milana Lisunova,†[a] Mahmoud Mahmoud,†[b] Neal Holland,[a] Zachary A. Combs,[a] Mostafa A. El-Sayed[b] and Vladimir V. Tsukruk*[a]

Received 19th April 2012, Accepted 7th June 2012
DOI: 10.1039/c2jm32450d

The fluorescence intensity of poly(*p*-phenyleneethynylene) (PPE) polymer separated from the surface of plasmonic silver nanocubes (47 nm AgNCs) is measured by varying the number of layers of polyvinyl pyrrolidone (PVPON) and polymethyl acrylic acid (PMAA), *n*. The shell thickness is sensitive to the solvent due to the formation of a solvent-sensitive hydrogen bonding network. The fluorescent behavior of the PPE on the core–shell PPE-(PVPON-PMAA)$_n$–AgNCs structures fabricated here was evaluated as a function of *n* as well as the nature of the surrounding solvent. Surprisingly, the fluorescence intensity of the outer PPE shell is found to increase dramatically (by more than an order of magnitude) as its separation from the nanoparticle surface increases and then decreases at a distance that depends upon the swelling behavior of the polymer shells. The distance for the highest fluorescence enhancement was found to be 20.0 nm and 24.0 nm, in water and ethanol respectively. The observed change in the fluorescence intensity of the PPE polymer with increasing its separation from the plasmonic surface is proposed to result from the interplay between a short range quenching mechanism and a relatively long-range plasmonic fluorescence enhancing mechanism. DDA calculations gave support to the significant contribution of the latter mechanism.

Introduction

Nanostructured metal cores coated with organic nanoshells are of great interest because of their potential applications in bio-analysis, as enhanced fluorescence labels, enhanced power conversion efficiency of dye-sensitized solar cells, optical bio-sensing, and plasmonic photocatalysis. Recent studies of the photophysical behavior of dyes assembled on metal nano-structures with core–shell morphology revealed that the inter-calation of the metal nanoparticles might significantly improve the photocurrent of dye-based sensitized solar cells (DSSCs).[1,2] A dye brightness enhancement by a factor of 30 due to the silica shell intercalation to the core has been shown by Ow *et al.* and explained by a change in the radiative properties of the dye in the vicinity of these nanostructures.[3] The increased fluorescence intensity of the dye-labeled microgels with a core–shell archi-tecture has been explained by the immobilization of the label molecules incorporated into the shell.[4]

In enhanced imaging approaches based on the fluorescence measurements, plasmonic nanoparticles are used to enhance the fluorescence intensity of the dye, in order to increase the imaging contrast and the resolution. Overall, the plasmon field intensity of the plasmonic nanoparticles decays on moving away from their surfaces.[5] The plasmonic nanoparticles have to be covered with an inert shell in order to prevent large intensity quenching due to electron and energy transfer, to lower the toxicity of the plasmonic nanoparticles, and to reduce their oxidation, espe-cially those made of silver. The most commonly used inert spacer coatings of the metallic nanoparticles are either rigid such as silica or soft as in the case of a hydrogel. However, the thickness of these mediating shells cannot be easily controlled. In the case of fluorescent molecules located at close proximity to a metal surface (that is within 5–8 nm) fluorescence quenching takes place,[5] mainly due to non-radiative energy transfer to the metallic nanoparticles.[6,7] At larger distances the enhancement starts to override the quenching mainly due to the domination of the surface plasmon resonance field of the silver nanoparticles. Several examples mentioned above show the effect of the shell utilization on the metal nanostructures on the optical properties of the fluorescence molecules located near the metal surfaces.[8–10] Despite a variety of modes of shell fabrication being suggested to date, the precise control of the shell thickness can be provided with very limited means in traditional approaches.

[a]*School of Materials Science and Engineering, Georgia Institute of Technology, Atlanta, Georgia 30332, USA. E-mail: vladimir@mse.gatech.edu*
[b]*School of Chemistry & Biochemistry (Laser Dynamic Lab.), Georgia Institute of Technology, Atlanta, Georgia 30332, USA*
† The two authors contributed equally.

The layer-by-layer (LbL) assembly is the most promising method for precise control of shell morphology and thickness which is hence explored in this study to control the distance between different components.[11–14] To this end, hydrogen bonded LbL assemblies containing water-soluble polymers and weak polyacids have received growing attention due to their high compliance, easy tenability, and responsiveness to environmental stimuli.[15–18] For instance, hydrogen bonding-based LbL films are highly pH sensitive and could be completely disintegrated at higher pH values while surviving quite well at lower ones.[16,17,19] In addition, LbL deposition enables precise control of the distance separating the photoactive units and the metal core and provides the flexibility for the facile integration of different fluorophores and other functionalities. Moreover, as was shown recently, coating cells by hydrogen bonded LbL shells reduces cytotoxicity and mediates cell growth.[18,20–23] The manipulation of these LbL films by changes in temperature or ionic strength gives the possibility to change the size and composition of the core–LbL shell structures and thus control energy transfer and fluorescent properties of conjugated polymers placed in the controlled proximity to the metal cores.

In this study, we prepared and studied core–shell nanostructures composed of a silver nanocube–polymer shell, which have strong plasmon field features resulting from the presence of sharp corners and edges. To create core–shell structures with controlled distance between the fluorescent coating and metal surface, silver nanocubes have been coated with hydrogen-bonded LbL shells with different thickness followed by the addition of the topmost PPE layer (Fig. 1). We demonstrated that the increasing thickness of the polymer shell as controlled by the number of LbL layers as well as the quality of solvent (water or ethanol) rapidly increases the fluorescence intensity of the topmost PPE layer then decreases it. This is proposed to result from a competition between a short range electron transfer fluorescence quenching mechanism and a longer range plasmonically driven enhancement of fluorescence.

Experimental

Polymethylacrylic acid (PMAA, molecular weight (M_w) 100 kDa), polyvinyl pyrrolidone (PVPON, M_w = 360 kDa), ethylene glycol (EG), sodium sulfide (Na_2S), and silver nitrate ($AgNO_3$) were purchased from Sigma-Aldrich. PPE with a molecular weight of 11 kDa was prepared as reported earlier.[24] Ultrapure water (Nanopure system) with a resistivity of 18.2 MΩ cm was used in all experiments.

Ag nanocubes are prepared by diol reduction of $AgNO_3$ in accordance with the known procedure.[25,26] Briefly, 35 mL of EG was heated to 150 °C for 1 h, followed by addition of 0.4 of PVPON dissolved in 5 mL of EG. The resulting solution was heated until the temperature rose to 150 °C. Na_2S (3 mM) dissolved in 0.4 mL of EG and 3.5 mL of 282 mM silver nitrate dissolved in EG were injected slowly into the reaction mixture. Silver ions were reduced completely after 15 minutes, producing Ag nanocubes. For purification of Ag nanocubes, 5 mL of the Ag nanocubes solution was diluted with water and centrifuged at 12 000 rpm for 5 minutes. The particles were then re-dispersed in water.

LbL assembly of $(PVPON\text{-}PMAA)_n$ multilayered shells has been performed according to the established procedure.[4,27] Briefly, 0.5 mg mL^{-1} of each polymer solution were prepared by dissolving the polymers in an aqueous buffer with pH adjusted to be 3.5. The typical deposition time on a single cycle was 15 min followed by three rinsing steps with an aqueous buffer solution (pH = 3.5) to remove excess free polymer. The polymer layers were coated one after the other. For nanoparticle suspensions, after each deposition step they were settled down by centrifugation at 4000 rpm for 4 min to remove the excess polymer. Deposition, rinsing and re-suspending steps were performed on a VWR analog vortex mixer at 4000 rpm.

Transmission electron microscopy (TEM) imaging of Ag nanocubes coated with polymers was performed on a JEOL 100CX operated at 100 kV. Before imaging, Ag nanocubes coated with polymers were drop cast on the carbon-former TEM grid (Electron Microscopy Sciences) and dried in air. AFM imaging of silver core–shell nanostructures was performed on a Bruker Icon system with a Nanoscope V controller using the tapping mode and scan assist regime in air.[28–30]

Surface potentials of the core–shell nanocubes in aqueous and ethanol solutions were measured on a Zetasizer Nano ZS (Malvern). Each value of zeta-potential was obtained under ambient conditions by averaging three independent measurements of 35 sub-runs each. Film thickness as well as the swelling ratio of the films in aqueous and ethanol solutions were obtained with an M-2000U spectroscopic ellipsometer (Woollam) by measuring film thickness in dry and swollen states. Prior to the measurements, samples were dried with a stream of nitrogen. UV-visible spectra were recorded using a UV-2450 spectrometer (Shimadzu). Experiments were carried out in 1.5 mL semi-microplastic cuvettes (PlastiBrand, Germany) with a 1 cm optical path. Fluorescence spectra of the dye-labeled core–shell nanoparticle dispersions were recorded at 90° on a RF-5301PC spectrofluorophotometer (Shimadzu). DDA calculations have been conducted using K. B. T. Draine and P. J. Flatau's DDA code, DDSCAT 6.1.

Results and discussion

LBL shells on Ag nanocubes with different number of layers

As synthesized, Ag nanocubes are capped with PVPON which facilitates the stability of the original solutions and the LbL assembly which started with the PMAA layer (Fig. 2). As judged

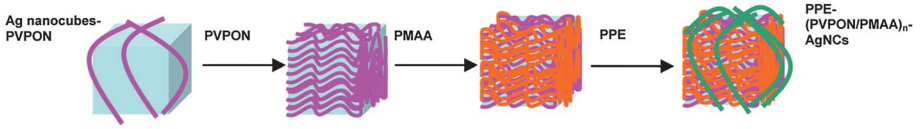

Fig. 1 Fabrication of Ag nanocubes with the topmost PPE coating separated by the LbL shell.

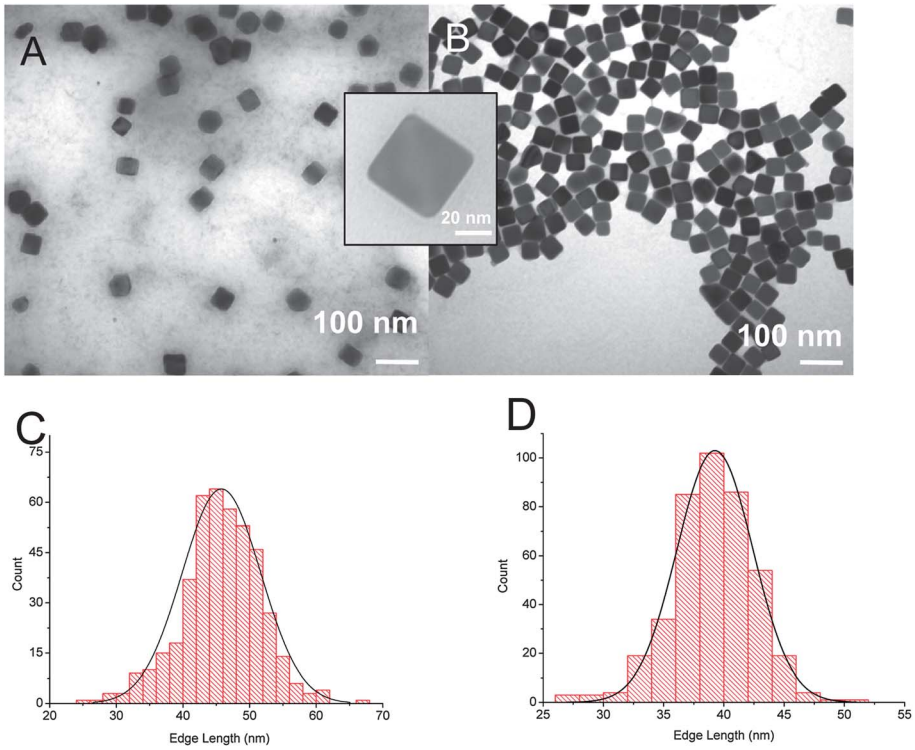

Fig. 2 TEM images of Ag nanocubes of 47 ± 5 nm (after single washing, (A), and multiple washing for LbL assembly, (B)) and corresponding size distribution (C and D).

from TEM measurements, the original Ag nanocubes are fairly uniform with an average dimension of 47 nm ± 5 nm. Multiple washing steps which are required for excessive surfactant removal before LbL assembly do not affect the effective dimensions of the silver cores as confirmed by statistical analysis of the nanocubes after different treatment steps (Fig. 2).

Examples of Ag nanocubes coated with different number of LbL polymer layers (3, 5, 9, and 11 bilayers of PVPON-PMAA) are shown in Fig. 3. The statistical evaluation of the TEM images revealed both individual nanocubes and mostly dimers and rarely trimers were observed after the LbL shell assembly. As a result, not only has the distance between the PPE coating and nanocube surfaces been changed but also the overall coating of aggregates increased in contrast to studies by Wustholz *et al.* in which the aggregates were coated by similar shells.[31] Moreover, as is clear from high-resolution TEM images, the corners of the silver nanocubes are slightly rounded due to the use of HCl to lower the pH. Indeed, it has been reported that HCl can round the corners of silver nanocubes due to a modest oxidation process.[32] Independently, AFM imaging has been conducted to confirm the uniformity of LbL polymer shells in the dry state. All images show a uniform distribution of coated nanocubes and homogeneous surfaces of the LbL shells and the topmost PPE coating (Fig. 4).

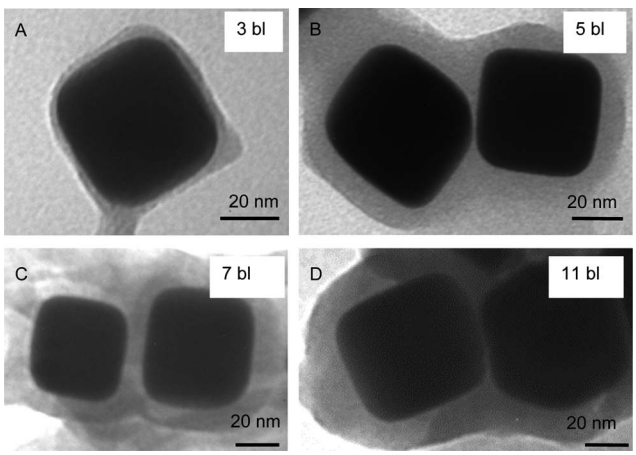

Fig. 3 TEM image of PPE-labeled Ag nanocubes coated with different LbL assembled bilayers of PVPON-PMAA: A, B, C and D are 3, 5, 7, and 11 polymer bilayers.

Based on the TEM evaluation the dry LbL shells in vacuum possess thicknesses of 1.5 ± 1, 5.0 ± 1.0, 10.0 ± 1.0, 15.0 ± 1.0, and 25.0 ± 1.0 nm for 1, 3, 5, 7, and 11 polymer bilayers, respectively (Table 1). In order to determine the actual thickness of the swollen shells in solution we conducted independent experiments by measuring the thickness of LbL films of identical composition deposited on a planar substrate in the dry state and in solvents (Table 1). The data show the thickness of the $(PVPON\text{-}PMAA)_n$ polymer film in the dry state under ambient conditions (vacuum, TEM data), and in the swollen state in two different solvents. The average thickness of the PVPON-PMAA bilayer in vacuum is around 2.2 nm and it increases to 2.5 nm per bilayer under ambient conditions due to residual water content (usually within 5–10%). Finally, in the aqueous buffer the LbL films are swollen by about 20% (slightly higher in water) with the average bilayer thickness reaching 3.0 nm that is close to the usual value for this polymer pair.[33,34]

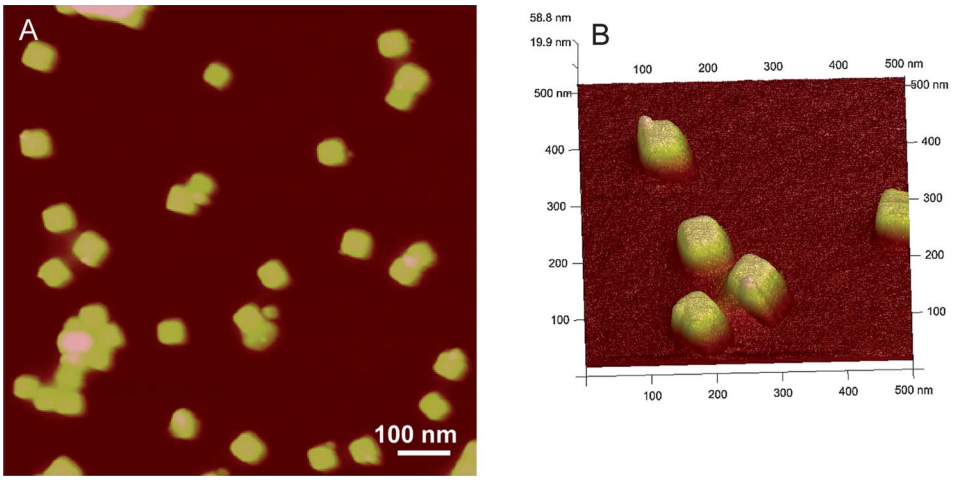

Fig. 4 AFM topography images of the silver nanocubes coated by one bilayer of the (PVPON-PMAA) at different scales. The Z-scale is 65 nm (A) and 60 nm (B).

Table 1 Thickness of LbL shells in the dry state and in the swollen state in aqueous buffer (pH = 3.5) and ethanol dispersion

Shell bilayer number	Shell thickness (dry) from TEM	Shell thickness (dry) from ellipsometry	Shell thickness (swollen) in aqueous dispersion	Shell thickness (swollen) in ethanol dispersion
1	1–2 nm	4 nm	5.3 nm	4.5 nm
3	5 nm	10 nm	13 nm	11 nm
5	10 nm	12 nm	15 nm	13 nm
7	15 nm	17 nm	21 nm	19 nm
9	20 nm	24 nm	28 nm	27 nm
11	25 nm	29 nm	34 nm	32 nm

Zeta-potential measurements confirm the assembly of differently charged polymer components on the silver nanocubes in different solvents (Fig. 5). Original silver nanocubes with PVPON coatings show a negative z-potential of −13 mV. Adding the first PMAA layer increases the negative potential due to the ionized phenolic groups of PMAA molecules with PVPON increasing the potential to slightly positive values. Overall, the characteristic saw-shape potential variation confirms a stable LbL assembly process (Fig. 5). The capping of shells with the topmost polycationic PPE coating results in the overall positively charged structures in both solutions thus confirming full recharge of the nanocubes.[34]

Optical properties of PPE-(PVPON-PMAA)$_n$–Ag nanocubes

Fig. 6 shows the UV extinction spectra of PPE-(PVPON-PMAA)$_n$–Ag nanocubes in aqueous and ethanol dispersions along with the PPE spectrum and DDA simulations of the nanocube extinction. The absorption maximum of the pure PPE solution in ethanol and aqueous buffer is located at 424 nm and 428 nm, respectively and can be associated with changes in the PPE conjugation in different solvents as well as the dielectric environment.[35,36] It is important to note that there is a significant overlap between the absorption peak of the PPE coating and silver nanocube plasmon absorption, which is one of the primary requirements for the efficient energy transfer for the donor–acceptor pair.

In contrast to the UV spectra of the original Ag nanocubes, that possess only an extinction peak around 464 nm, the PPE-(PVPON-PMAA)$_n$–Ag nanocubes exhibit two broad extinction peaks. The main peak is similar to that observed for the original silver nanocubes (within 440–470 nm) but the additional lower intensity extinction band is centered around 600 nm.

In order to analyze these changes, we carried out DDA simulations for both a 40 ± 5 nm single nanocube and a nanocube dimer at a separation distance of 10 nm which mimics that observed for aggregated core–shell nanocubes (Fig. 6D). The dielectric properties of the surrounding medium were taken to be for the mixture of polymer shells and water or ethanol (replacing water by ethanol did not affect the calculation). The DDA simulations showed that individual Ag nanocubes should possess multiple extinction plasmon peaks which are red-shifted as compared with the experimental data. Such differences can be attributed to variations of shape, chemical composition and dielectric environment as well as electrostatic coupling[37–40] and edge rounding effects.[41]

Based on these DDA calculations, the two extinction peaks centered at ~460 and ~600 nm, for the PPE-(PVPON-PMAA)$_n$–Ag nanocubes, can be assigned to different SPR bands of core nanocubes. The peak at 460 nm corresponds to an individual Ag nanocube and a peak at 580 nm can be assigned to plasmonic coupling of dimers. In a related study, Yang *et al.*[42] explained the appearance of the SPR coupling bands by aggregation of silver nanoparticles to the linear-chain and 3D aggregates. Wustholz *et al.* considered the effect of the specific type of the nanoparticle assembling (dimers and trimers) on the SPR spectrum and concluded that local arrangement defines the SPR appearance similarly to that observed here.[31] The ratio between the SPR peak intensities can be related to the ratio of individual and dimer nanocubes. This ratio increases as the number of bilayers of LbL shells increases. The dimer nanoparticle aggregation becomes predominant ($I_{580}/I_{460} > 1$) for thicker LbL shells with 5 and 9 bilayers in aqueous and ethanol dispersions, respectively with a higher level of aggregation observed for the water dispersion.

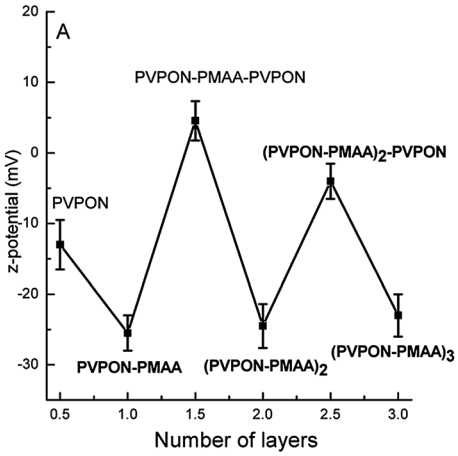

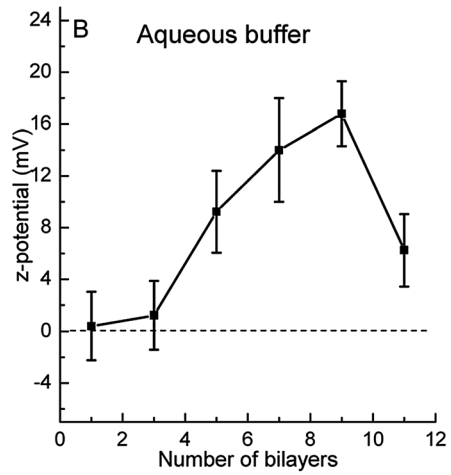

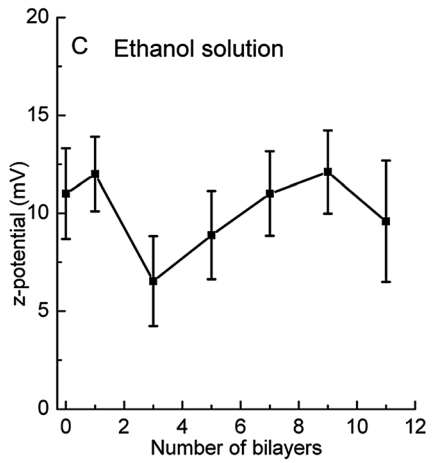

Fig. 5 Zeta-potential variation during LbL shell formation on silver nanocubes in aqueous solution (A) and during PPE assembling on the Ag nanocubes in aqueous (B) and ethanol dispersions (C).

Fluorescence emission of PPE-(PVPON-PMAA)$_n$–Ag nanocubes

The confocal fluorescence imaging of the dispersed PPE-(PVPON-PMAA)$_n$–Ag nanocubes, measured at the 488 nm excitation wavelength, confirmed the PPE coating of nanocubes and their aggregates (Fig. 7).

The corresponding fluorescent spectra of the PPE-(PVPON-PMAA)$_n$–Ag nanocubes at different shell thicknesses (different separations between nanocubes and the topmost PPE coating) at 450 nm excitation wavelength show characteristic features of both silver nanocubes and the topmost PPE coating with blue-shifting from 474 nm to 460 nm in ethanol caused by changes in conjugation length (Fig. 8). The UV extinction peaks of the PPE-(PVPON-PMAA)$_n$–AgNCs with different shell thickness are modestly blue shifted confirming modest aggregation (Fig. 9). The variation of the UV extinction peaks of the metal-core–shell nanoparticles with changing the shell thickness was also reported recently by Vanderkooy *et al.*[43] On the other hand, the positions of the fluorescent peaks remain virtually unchanged thus indicating unchanged conjugation properties of the topmost PPE coating (Fig. 9).

Remarkably, the experimental results show the non-monotonous variation of the fluorescence intensity of the PPE coating separated from the Ag nanocube by LbL polymer shells with different thickness (Fig. 10). A dramatic increase in fluorescence with increasing separation was observed for the thinnest shells with the number of bilayers below 9. However, this rise in fluorescent intensity is replaced by a significant drop for the PPE-(PVPON-PMAA)$_n$–AgNCs with the thickest shells with the thickness in the swollen state reaching 30–35 nm (Table 1). The optimum separation distance at which the fluorescence intensity increases 11 fold in water and 26 fold in ethanol was found to be 20 nm and 24.0 nm, respectively. It is worth noting that the minor changes in specific surface areas associated with shell thickness increase (PPE concentration effect) such as that observed by Xie *et al.*[44] cannot explain the dramatic effects observed here.

On the other hand, the observed variation of the fluorescent intensity is in good agreement with the theoretical estimation given by Tovmachenko *et al.*[45] where an optimal separation distance for an enhanced fluorescence of 20–30 nm was predicted. According to Liaw *et al.*[46] the maximum enhancement factor as well as thickness of the insulating shells vary with the size of the nanoparticles and should fall in the range of 20–25 nm for 50–60 nm nanocubes. The difference in the enhancement behavior for aqueous and non-aqueous (ethanol) dispersions can be associated with the variation in the dielectric constant of the ambient environment and different swelling of the polymer shells (Table 1). Such an ability to tune the fluorescence intensity of the PPE-(PVPON-PMAA)$_n$–AgNCs by varying the thickness of the LbL shells as well as its swelling in different solvents is critically important for the design of dye-based solar and photovoltaic cells, as well as biosensing materials with controllable brightness.

Several important factors might affect the fluorescent intensity of the PPE coatings on Ag nanocubes.[47–50] The most important contributions are related to the plasmon field which enhances the fluorescence and the quenching and self-quenching phenomena.[51,52] For instance, gold nanoparticles can quench the fluorescence emission of PPE chains with quenching efficiency which is independent of the overlap between the SPR and the fluorescence spectrum, suggesting an electron transfer mechanism.[53] The quenching phenomena for PPE-(PVPON-PMAA)$_n$–AgNCs studied here can be caused by the distance-controlled energy transfer between the PPE coating and the Ag

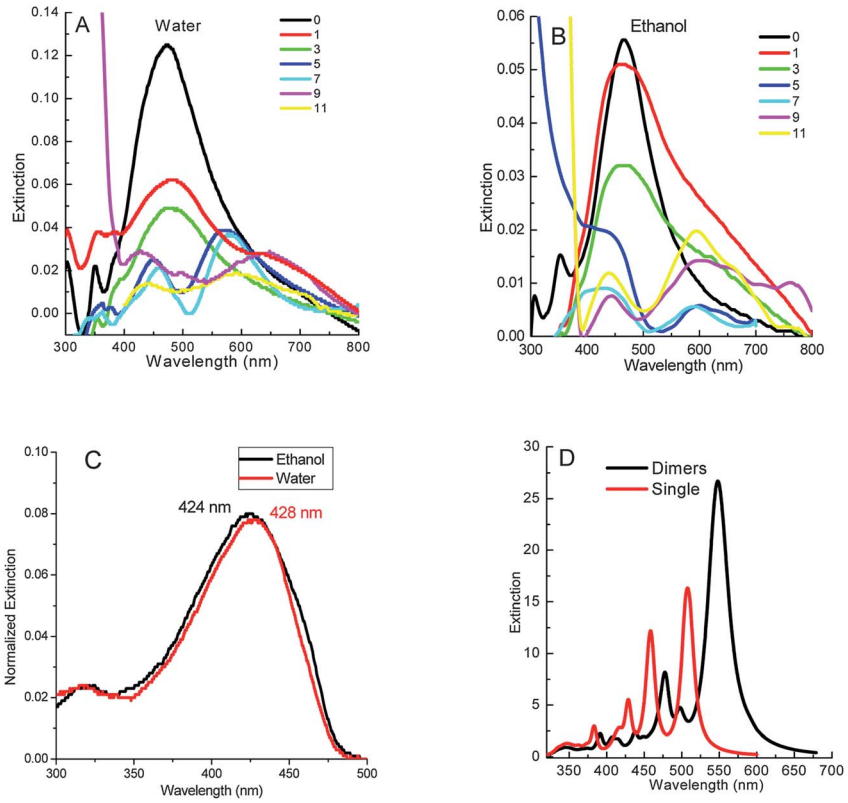

Fig. 6 UV extinction spectra of Ag nanocubes coated with the PPE coating on Ag nanocubes with $(PVPON\text{-}PMAA)_n$ shells: (A) in water and (B) ethanol. (C) The absorption spectrum of PPE in water and ethanol. (D) The SPR spectrum of a 40 nm Ag nanocube and a pair of Ag nanocubes placed at a 10 nm separation gap coated with PVPON-PMAA, calculated by the DDA simulation.

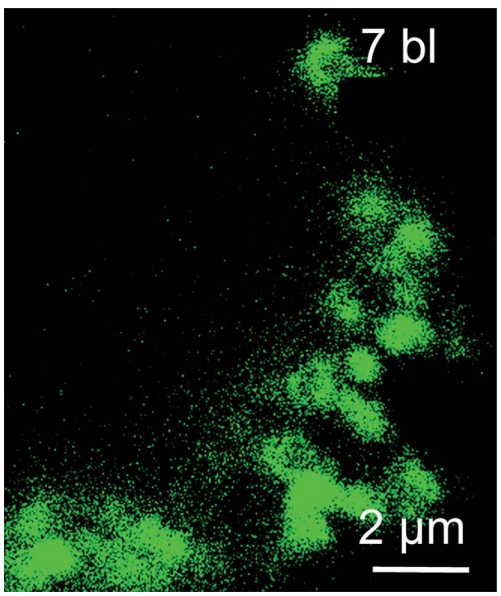

Fig. 7 Confocal images of the PPE-$(PVPON/PMAA)_7$–AgNCs in ethanol.

nanocubes.[52] In fact, the fluorescence spectra of the PPE coating overlap with the SPR peaks of the individual and dimer Ag nanocubes. The energy and electron transfer quenching mechanisms can occur as long as the PPE coating is close to the silver surface. The second mechanism could be static quenching resulting from the Columbic interactions between the Ag nanocube shell elements with localized charges able to quench the fluorescence of the topmost PPE coating.[52]

In order to evaluate the role of the plasmon field on the fluorescence enhancement, we carried out DDA simulation for the plasmon field distribution as a function of distance because the plasmon field intensity is responsible for the fluorescence enhancement (Fig. 11). Note that the plasmon field was calculated as a function of distance from the surface of the nanocube. The DDA calculation demonstrates the plasmon field contour of individual and dimer Ag nanocubes placed at a 10 nm separation distance. The propagation of light is along the *x*-direction, while the light is polarized along the *y*-direction, and the plasmon field propagates perpendicular to the plane of the particle.

As is clear from these calculations, the distribution of the plasmonic field differs significantly for nanocube dimers in comparison with individual nanocubes with an additional local increase observed in the middle of the edges at adjacent facets (Fig. 11).[54] Sections of the plasmon field show dramatic exponential decay as the thickness of the polymer shell increases above 5 nm which continues to a 15–25 nm separation distance. Moreover, different plasmon modes might overlap differently with the excitation source which results in different fluorescence enhancement modes. It well known that the plasmon field of the single plasmonic nanoparticle is stronger than that of its pair and

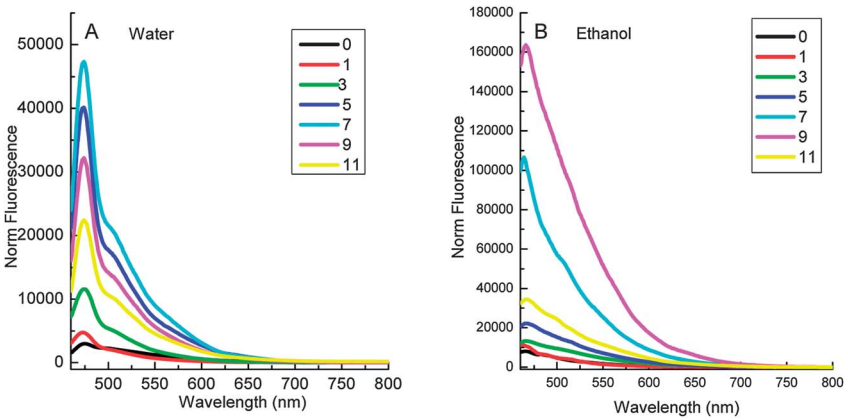

Fig. 8 The fluorescence spectra of PPE-(PVPON/PMAA)$_n$–AgNCs as a function of the number of LbL bilayers in aqueous (A) and ethanol (B) dispersions.

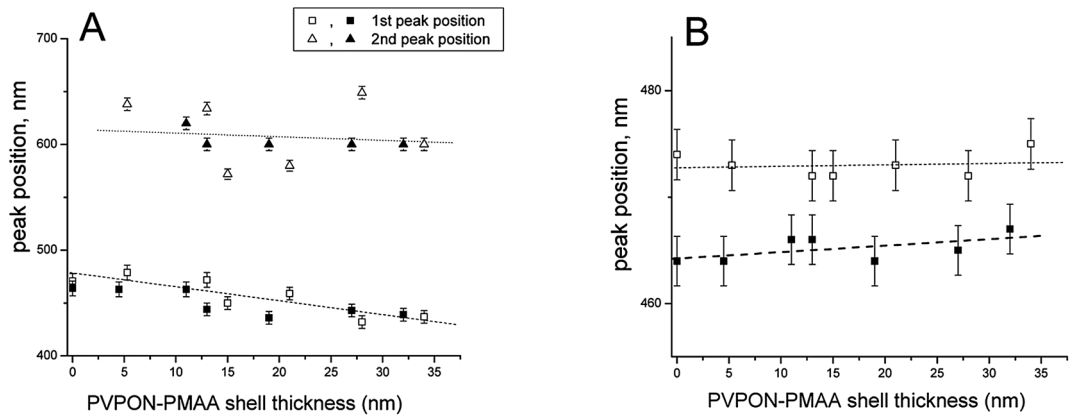

Fig. 9 Positions of UV-extinction peaks (A) and fluorescent emission peaks (B) for PPE-(PVPON/PMAA)$_n$–AgNCs for different numbers of LbL bilayers in ethanol (filled symbols) and aqueous dispersions (hollow symbols).

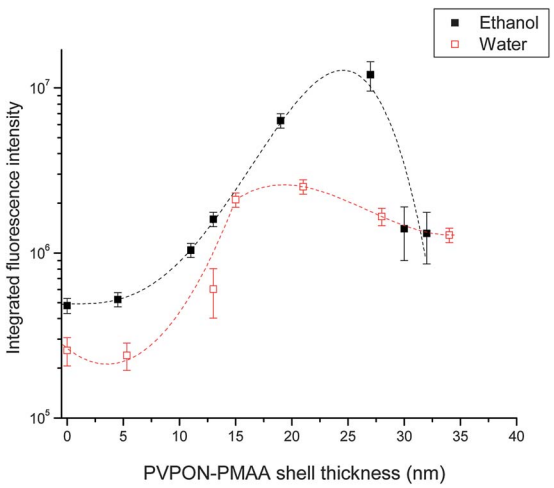

Fig. 10 The fluorescent intensity of the PPE-(PVPON/PMAA)$_n$–AgNCs with different number of LbL bilayers (shell thickness) normalized to the nanocube concentration.

the density of this plasmon field is usually highest in the region between the nanoparticle pairs.[55,56] This behavior is true when the plasmon field is calculated at the maximum LSPR peak. In our fluorescence measurement the 450 nm wavelength was used for the excitation of the PPE fluorescent polymer shell. However, the DDA simulation of the plasmon field at 450 nm showed that the field of the single silver nanocube is stronger than the dimer. This result suggests that the enhancement of fluorescence by the single nanocube in the vicinity of the surface might be higher than that by the dimer.

The unusual tremendous non-monotonic variation of PPE fluorescence observed here can be related to the competing balance of quenching in the vicinity of the metal surface leading to decreasing fluorescence intensity and the plasmon field enhancement leading to the increasing fluorescence intensity. At the smallest separation between the nanocube surface and PPE coating (2–3 nm) the fluorescent quenching dominates due to the proximity of PPE chains to the metal surface and high mobility of ions in the swollen shells. Further separation of PPE chains and the metal surface results in significant decrease in quenching thus promoting increased fluorescent intensity at greater separation distances. On the other hand, plasmon field intensity is still high at these distances thus further promoting the increase in fluorescent intensity for the separation increasing from 3 nm to 15 nm. Finally, crossover is reached at larger separation (20–25 nm depending upon the quality of the solvent) where

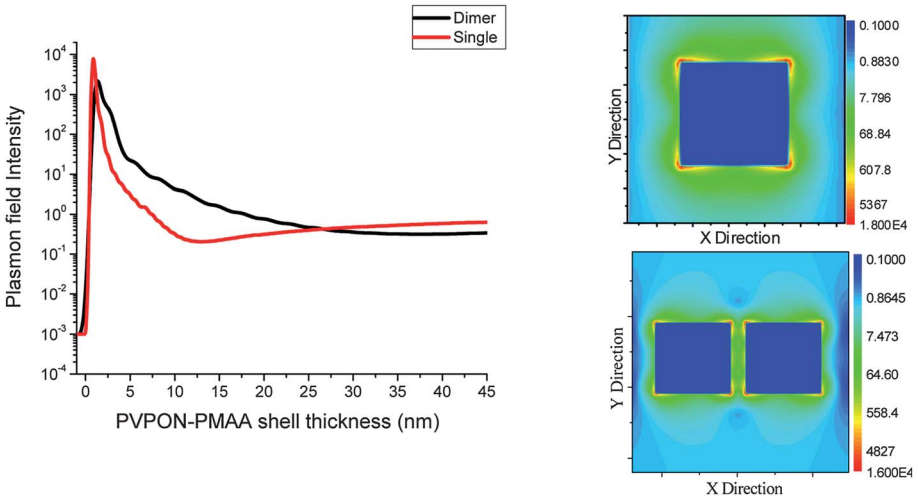

Fig. 11 The relationship between the plasmon field intensity and the distance from the surface of the Ag nanocube, single and dimers (left). The plasmon field contour of both single and dimer nanocubes (right).

quenching diminishes and the plasmonic enhancement of the fluorescent intensity becomes insignificant.

Acknowledgements

This work was supported by the U.S. Department of Energy, Office of Basic Energy Sciences, Division of Materials Sciences and Engineering under award # DE-FG02-09ER46604. Z. A. Combs thanks the National Defense Science and Engineering Graduate (NDSEG) Fellowship, 32 CFR 168a.

References

1 J. Qi, X. Dang, P. T. Hammond and A. M. Belcher, *ACS Nano*, 2011, **5**(9), 7108–7116.
2 M. D. Brown, T. Suteewong, R. S. S. Kumar, V. D'innocenzo, A. Petrozza, M. M. Lee, U. Wiesner and H. J. Snaith, *Nano Lett.*, 2010, **11**(2), 438–445.
3 H. Ow, D. R. Larson, M. Srivastava, B. A. Baird, W. W. Webb and U. Wiesner, *Nano Lett.*, 2005, **5**(1), 113–117.
4 C. Graf, W. Schartl, K. Fischer, N. Hugenberg and M. Schmidt, *Langmuir*, 1999, **15**(19), 6170–6180.
5 G. Schneider and G. Decher, *Nano Lett.*, 2006, **6**(3), 530–536.
6 J. I. Gersten, *Chem. Phys. Lett.*, 1984, **104**(1), 31–37.
7 E. Dulkeith, M. Ringler, T. A. Klar and J. Feldmann, *Nano Lett.*, 2005, **5**(4), 585–589.
8 Y. Zhang, K. Aslan, M. J. R. Previte and C. D. Geddes, *Chem. Phys. Lett.*, 2008, **458**, 147–151.
9 Z. Wang, Z. Chen, Z. Lan, X. Zhai, W. Du and Q. Gong, *Appl. Phys. Lett.*, 2007, **90**, 1511190–1511193.
10 I. Delfino and S. Cannistraro, *Biophys. Chem.*, 2009, **139**, 1–7.
11 G. Decher and J. B. Schlenoff, *Multilayer Thin Films – Sequential Assembly of Nanocomposite Materials*, Wiley-VCH, 2003.
12 D. Lee, R. E. Cohen and M. F. Rubner, *Langmuir*, 2005, **21**, 9651–9659.
13 C. Jiang and V. V. Tsukruk, *Adv. Mater.*, 2006, **18**, 829–840.
14 R. Choi, F. A. Suntivich, C. V. Plamper, Synatschke, A. H. E. Müller and V. V. Tsukruk, *J. Am. Chem. Soc.*, 2011, **133**, 9592–9606.
15 V. Khutoryanskiy, *Int. J. Pharm.*, 2007, **334**, 15–26.
16 E. Kharlampieva and S. A. Sukhishvili, *J. Macromol. Sci., Part C: Polym. Rev.*, 2006, **46**, 377–395.
17 P. Lavalle, J. C. Voegel, D. Vautier, B. Senger, P. Schaaf and V. Ball, *Adv. Mater.*, 2011, **23**, 1191–1221.
18 J. E. Quinn and F. Caruso, *Aust. J. Chem.*, 2005, **58**, 442–446.
19 S. A. Sukhishvili and S. Granick, *Macromolecules*, 2002, **35**, 301–310.
20 V. Kozlovskaya, S. Harbaugh, I. Drachuk, O. Shchepelina, N. Kelley-Loughnane, M. Stone and V. V. Tsukruk, *Soft Matter*, 2011, **7**, 2364–2372.
21 J. L. Carter, I. Drachuk, S. Harbaugh, N. Kelley-Loughnane, M. Stone and V. V. Tsukruk, *Macromol. Biosci.*, 2011, **11**, 1244–1253.
22 J. T. Wilson, W. Cui, V. Kozlovskaya, E. Kharlampieva, D. Pan, Z. Qu, V. R. Krishnamurthy, J. Mets, V. Kumar, J. Wen, Y. Song, V. V. Tsukruk and E. L. Chaikof, *J. Am. Chem. Soc.*, 2011, **133**, 7054–7064.
23 C. Ye, O. Shchepelina, R. Calabrese, I. Drachuk, D. L. Kaplan and V. V. Tsukruk, *Biomacromolecules*, 2011, **12**, 4319–4325.
24 M. A. Mahmoud, A. J. Poncheri, R. L. Phillips and M. A. El-Sayed, *J. Am. Chem. Soc.*, 2010, **132**, 2633–2641.
25 Y. G. Sun and Y. N. Xia, *Science*, 2002, **298**, 2176–2179.
26 M. A. Mahmoud, C. E. Tabor and M. A. El-Sayed, *J. Phys. Chem. C*, 2009, **113**, 5493–5501.
27 V. Kozlovskaya, E. Kharlampieva, B. P. Khanal, P. Manna, E. R. Zubarev and V. V. Tsukruk, *Chem. Mater.*, 2008, **20**, 7474–7485.
28 V. V. Tsukruk and D. H. Reneker, *Polymer*, 1995, **36**, 1791–1808.
29 M. E. McConney, S. Singamaneni and V. V. Tsukruk, *Polym. Rev.*, 2010, **50**, 235–286.
30 V. V. Tsukruk, Z. Huang, S. A. Chizhik and V. V. Gorbunov, *J. Mater. Sci.*, 1998, **33**, 4905–4909.
31 K. L. Wustholz, A. I. Henry, J. M. McMahon, R. G. Freeman, N. Valley, M. E. Piotti, M. J. Natan, G. C. Schatz and R. P. Van Duyne, *J. Am. Chem. Soc.*, 2010, **132**, 10903–10910.
32 J. M. McLellan, A. Siekkinen, J. Y. Chen and Y. N. Xia, *Chem. Phys. Lett.*, 2006, **427**, 122–126.
33 M. O. Lisunova, I. Drachuk, O. Shchepelina, K. Anderson and V. V. Tsukruk, *Langmuir*, 2011, **27**, 11157–11165.
34 V. Kozlovskaya, E. Kharlampieva, I. Drachuk, D. Cheng and V. V. Tsukruk, *Soft Matter*, 2010, **6**, 3596–3608.
35 T.-Q. Nguyen, V. Doan and B. J. Schwartz, *J. Chem. Phys.*, 1999, **110**, 4068–4079.
36 T.-Q. Nguyen, R. C. Kwong, M. E. Thompson and B. J. Schwartz, *Appl. Phys. Lett.*, 2000, **76**, 2454–2457.
37 U. Kreibig and M. Vollmer, *Optical Properties of Metal Clusters*, Springer, Berlin, 1995.
38 L. S. Slaughter, Y. P. Wu, B. A. Willingham, P. Nordlander and S. Link, *ACS Nano*, 2010, **4**, 4657–4666.
39 C. Tabor, D. Van Haute and M. A. El-Sayed, *ACS Nano*, 2009, **3**, 3670–3678.
40 A. M. Funston, C. Novo, T. J. Davis and P. Mulvaney, *Nano Lett.*, 2009, **9**, 1651–1658.
41 N. Grillet, D. Manchon, F. Bertorelle, C. Bonnet, M. Broyer, E. Cottancin, J. Lermé, M. Hillenkamp and M. Pellarin, *ACS Nano*, 2011, **5**(12), 9450–9462.

42 Y. Yang, J. Shi, T. Tanaka and M. Nogami, *Langmuir*, 2007, **23**, 12042–12047.
43 A. Vanderkooy, Y. Chen, F. Gonzaga and M. A. Brook, *ACS Appl. Mater. Interfaces*, 2011, **3**, 3942–3947.
44 F. Xie, M. S. Baker and E. M. Goldys, *Chem. Mater.*, 2008, **20**, 1788–1797.
45 O. G. Tovmachenko, C. Graf, D. J. van den Heuvel, A. van Blaaderen and H. C. Gerritsen, *Adv. Mater.*, 2006, **18**, 91–95.
46 J. W. Liaw, C. L. Liu, W. M. Tu and C. S. Sun, *J. Quant. Spectrosc. Radiat. Transfer*, 2011, **112**, 893–900.
47 G. Schneider and G. Decher, *Nano Lett.*, 2006, **6**(3), 530–536.
48 J. I. Gersten, *Chem. Phys. Lett.*, 1984, **104**(1), 31–37.
49 E. Dulkeith, M. Ringler, T. A. Klar and J. Feldmann, *Nano Lett.*, 2005, **5**(4), 585–589.
50 Z. Fei, L. Ye and L. Zhi-Yuan, *Chin. Phys. B*, 2011, **20**(3), 1–8.
51 M. A. Mahmoud and M. A. El-Sayed, *J. Phys. Chem. C*, 2011, **115**, 12726–12735.
52 C. Fan, S. Wang, J. W. Hong, G. C. Bazan, K. W. Plaxco and A. J. Heeger, *Proc. Natl. Acad. Sci. U. S. A.*, 2003, **100**, 6297–6301.
53 T. M. Swager, *Acc. Chem. Res.*, 1998, **31**, 201–207.
54 F. Le, D. W. Brandl, Y. A. Urzhumov, H. Wang, J. Kundu, N. J. Halas, J. Aizpurua and P. Nordlander, *ACS Nano*, 2008, **2**, 707–718.
55 A. J. Haes, C. L. Haynes, A. D. McFarland, G. C. Schatz, R. P. van Duyne and S. Zou, *MRS Bull.*, 2005, **30**, 368–375.
56 A. J. Haes, S. Zou, G. C. Schatz and R. P. Van Duyne, *J. Phys. Chem. B*, 2004, **108**, 6961–6968.